Published in final edited form as:
Neurobiol Aging. 2008 September ; 29(9): 1296–1307. doi:10.1016/j.neurobiolaging.2007.03.007.

Stereologic estimates of total spinophilin-immunoreactive spine number in area 9 and the CA1 field: relationship with the progression of Alzheimer's disease

Afia Akram[a,b], **Daniel Christoffel**[a], **Anne B. Rocher**[a], **Constantin Bouras**[a,e], **Enikö Kövari**[e], **Daniel P. Perl**[c], **John H. Morrison**[a,d], **François R. Herrmann**[f], **Vahram Haroutunian**[b], **Panteleimon Giannakopoulos**[e], and **Patrick R. Hof**[a,d*]

[a]*Department of Neuroscience, Mount Sinai School of Medicine, New York, NY 10029* [b]*Department of Psychiatry, Mount Sinai School of Medicine, New York, NY 10029* [c]*Department of Pathology (Neuropathology), Mount Sinai School of Medicine, New York, NY 10029* [d]*Department of Geriatrics and Adult Development, Mount Sinai School of Medicine, New York, NY 10029* [e]*Department of Psychiatry, University of Geneva, School of Medicine, Geneva, Switzerland* [f]*Department of Rehabilitation and Geriatrics, University of Geneva, School of Medicine, Geneva, Switzerland*

Abstract

The loss of presynaptic markers is thought to represent a strong pathologic correlate of cognitive decline in Alzheimer's disease (AD). Spinophilin is a postsynaptic marker mainly located to the heads of dendritic spines. We assessed total numbers of spinophilin-immunoreactive puncta in the CA1 and CA3 fields of hippocampus and area 9 in 18 elderly individuals with various degrees of cognitive decline. The decrease in spinophilin-immunoreactivity was significantly related to both Braak neurofibrillary tangle (NFT) staging and clinical severity but not Aβ deposition staging. The total number of spinophilin-immunoreactive puncta in CA1 field and area 9 were significantly related to MMSE scores and predicted 23.5% and 61.9% of its variability. The relationship between total number of spinophilin-immunoreactive puncta in CA1 field and MMSE scores did not persist when adjusting for Braak NFT staging. In contrast, the total number of spinophilin-immunoreactive puncta in area 9 was still significantly related to the cognitive outcome explaining an extra 9.6% of MMSE and 25.6% of the Clinical Dementia Rating scores variability. Our data suggest that neocortical dendritic spine loss is an independent parameter to consider in AD clinicopathologic correlations.

Keywords

Alzheimer's disease; cognition; synapses; tangles

*Correspondence to: Patrick R. Hof, Department of Neuroscience, Box 1065, Mount Sinai School of Medicine, One Gustave L. Levy Place, New York, NY 10029, USA, Phone: +1-212-659-5904; Fax: +1-212-849-2510; E-mail: patrick.hof@mssm.edu.

None of the authors declare an actual or potential conflict of interest.

1. Introduction

Alzheimer's disease (AD) is a progressive, degenerative disorder of the central nervous system. The major hallmarks of AD include the presence of extracellular amyloid deposits and intracellular neurofibrillary tangles (NFT) [2,4,19,70,82]. Several studies have shown that in addition to these traditionally described lesions, AD is characterized by selective neuronal loss [30,72], severe and early loss of synapses [15,16,24,45,59], and synaptic pathology [41,44]. Early immunocytochemical studies indicated an average 45% decrease in presynaptic terminal density in the AD neocortex [44,45,76]. Quantitative morphometric study of temporal and frontal cortical biopsies performed within an average of 2 to 4 years from the onset of clinical AD revealed 25 to 35% decrease in the numerical density of synapses and 15 to 35% decrease in the number of synapses per cortical neuron [15]. In terms of clinicopathologic correlations, much of the previous work has focused on loss of presynaptic markers such as synaptophysin [18,42,43,58,68,71]. The contribution of Terry and collaborators first implied that severity of AD is more robustly related to synapse loss than amyloid plaques, NFT densities, degree of neuronal loss, or extent of cortical gliosis [71]. In particular, they postulated that synaptophysin decrease in the prefrontal cortex is the major correlate of cognitive deficits, explaining about 70% of the global psychometric test variability [71]. Recent reports revealed synaptophysin immunoreactivity reduction in NFT-containing neurons in the hippocampus and association cortices in minimal cognitive impairment and early AD, pointing to the relationship between NFT formation and loss of presynaptic markers [8,28,42,68]. However, estimates of synaptic loss in these studies relied upon density measures and were based on two unwarranted assumptions, namely that the size of the region under analysis remains constant across diagnostic groups and that synaptic size does not change [13,58,80].

In contrast to presynaptic markers, AD changes in postsynaptic structures have been less studied. Although postsynaptic components are thought to be affected in early-onset AD [14, 65], few studies have explored in humans the status of dendritic spines in brain aging. Spines are dynamic structures that are the proposed site of synaptic plasticity underlying learning and memory [34,49,62]. Because of the distance of dendritic extent from the soma, dendritic spines may be particularly vulnerable to incipient degenerative processes that disrupt intracellular signaling and synaptic functions. It has been hypothesized that alterations in synaptic activity can cause morphologic changes in dendritic spines [27,40,46]. Conversely, morphologic changes in dendritic spines [51,64,83] have profound effects on the electrical and biochemical properties of synapses [17,67], and may regulate the efficacy of synaptic transmission [83].

Spinophilin, also called neurabin II [56], is a synaptic protein implicated in spine formation and synaptic transmission in different types of dendritic spines and at excitatory and some inhibitory postsynaptic sites on dendritic shafts [50,53]. Spinophilin displays a remarkably distinct localization to the heads of majority of dendritic spines in all brain regions examined, although the concentration per spine is regionally and locally variable. Spinophilin immunoreactivity has been shown to be intense in the majority of dendritic spines of rat hippocampus [1]. It is present in about 93% of the dendritic spines in rhesus monkey hippocampus [25], but sparsely distributed in other portions of the dendrites, making it an excellent marker for quantitative assessment of spine numbers [25]. In order to explore the role of dendritic spine loss in cognitive decline, we performed a stereological analysis of spinophilin-immunoreactive puncta in the CA1 and CA3 fields of the hippocampus and area 9 in 12 elderly individuals prospectively assessed with the Mini Mental State Examination (MMSE) and Clinical Dementia Rating (CDR) scale.

2. Methods

2.1. Patients

The brains from 18 elderly patients, presenting with either normal aging or with various degrees of cognitive impairment were obtained at autopsy within 30 hours of death. Clinical data were obtained from the medical records of the patients and the neuropathologic evaluation from the Departments of Geriatrics and Psychiatry, University of Geneva School of Medicine, Geneva, Switzerland, and the Department of Psychiatry, Mount Sinai School of Medicine, New York, USA (Table 1). All cases underwent neuropsychological assessment within the last 6 months prior to their death and a Mini-Mental State Examination score [21] (MMSE) was available for all of them (Table 1). All cases were further classified according to the Clinical Dementia Rating score [47] (CDR; CDR 0, $n = 6$, mean age = 89.8 years; CDR 0.5, $n = 5$, mean age = 77.6 years; CDR 1, $n = 1$, age = 87.0 years; CDR 2, $n = 3$, mean age = 88.7 years; CDR 3, $n = 3$, mean age = 87.7 years). The CDR is a validated scale that is widely used for the clinical staging of dementia [35]. It assigns cognitive function to five levels defined as no dementia (CDR 0), questionable dementia (CDR 0.5), mild dementia (CDR 1), moderate dementia (CDR 2) and definite dementia (CDR 3). Gender and age distribution of the cases according to CDR score are listed in Table 1. Cases with stroke history or other central nervous system disorders (i.e., tumors, inflammation, Parkinson's disease, Lewy body disease) were excluded from the present study. All procedures involving the use of postmortem human brain were conducted after written consent of the next of kin was obtained, and were approved by the relevant ethics committees at the University of Geneva School of Medicine and Mount Sinai School of Medicine.

2.2. Tissue processing and immunocytochemistry

All brains were hemisected at autopsy and the right cerebral hemispheres were fixed in 4% paraformaldehyde for up to 4 weeks. The entire superior frontal gyrus and the whole hippocampus and parahippocampal gyrus were dissected out, placed in phosphate buffer and blocked at regular intervals using a specially designed multi-blade knife [54]. This knife is composed of a series of disposable microtome blades, whose number can be modified according to the size of the tissue block, secured with brass machine screws and separated by washers of variable size depending on which slab thickness is appropriate. Depending on the case, this results in a total of 10–16 blocks of equal thickness that comprise the entire rostrocaudal extent of the superior frontal gyrus and therefore, represent an exhaustive sample [54]. In the case of the hippocampus 7–10 blocks were obtained. These slabs were numbered in order, taking note of the rostral surface of each block. Alternate blocks were either processed for paraffin embedding, or were placed in graded sucrose and cut on a Vibratome. A random number determined whether the odd numbered or even numbered blocks would be subjected to Vibratome sectioning or be available for paraffin embedding. The paraffin-embedded blocks were reserved for neuropathologic evaluation whereas the alternate blocks were employed for the stereologic analyses. Routine neuropathologic assessment including visualization of NFT, neuritic plaques and neuropil threads was made on 7 μm-thick sections from the paraffin-embedded blocks that were stained with modified Bielschowsky and Gallyas methods [74]. The visualization of Aβ protein deposits was performed using a monoclonal antibody 4G8 (ascite fluid) directed against the sequence 17–24 of amyloid peptide as previously described [23]. Antibody 4G8 was used to detect deposits made of Aβ1–40 or Aβ1–42, because its recognized epitope does not include the carboxy-terminus and is common to all species of amyloid peptide [79]. Five fields from these sections were sampled at 20x magnification for diagnostic purposes. Subsequently, all cases were classified neuropathologically according to Braak-NFT staging system [4]. Aβ-protein deposition staging was performed according to the amyloid nomenclature proposed by Thal and collaborators [73]. The Vibratome blocks were cut at 50 μm and processed for immunostaining and histochemistry. Sections were kept in strict

anatomical order in buffer and any gap in the series was noted. Special care was made to lose a minimal amount of tissue at the interface between blocks. Thus, depending on the region 4–8 sections (1 per alternate block resulting in a 1:120 series) could be analyzed to sample exhaustively the region considered [54]. The sections sampled for stereology were then labeled with an antibody against spinophilin and used for further analysis.

For spinophilin visualization, sections were thoroughly rinsed in 0.01 M PBS containing 0.3% Triton X-100 and then incubated in a blocking buffer containing 0.3% Triton X-100, 0.1% cold water fish gelatin (Electron Microscopy Sciences, Fort Washington, PA), 0.5% bovine serum albumin (Sigma, St. Louis, MO), and 5% normal goat serum (Vector Laboratories, Burlingame, CA) for 1 hour at room temperature. Free-floating sections were incubated with a fully characterized rabbit anti-spinophilin primary antibody (generously provided by Drs Paul Greengard and Patrick Allen [1,53]) diluted 1:240,000 in the above-described blocking buffer) for 72 hours at 4°C, washed, and incubated in secondary antibody (goat anti-rabbit IgG, ultrasmall EM grade; Electron Microscopy Sciences, Fort Washington, PA) in the above-described diluent for 3 hours at room temperature. The secondary antibody was used at a dilution of 1:100 in PBS containing 0.3% Triton X-100. Sections were washed and postfixed with 2% glutaraldehyde in PBS and rinsed with distilled water. The silver enhancement reagent was prepared by mixing equal amounts of Aurion R-Gent Developer Aurion and Enhancer (Electron Microscopy Sciences, Fort Washington, PA) before use. Silver Enhancement was performed for 15–25 minutes at room temperature. After washing, the sections were mounted, dehydrated through ascending series of ethanol and xylene, and coverslipped with Biomount mounting medium (Electron Microscopy Sciences) [25,69]. This spinophilin antibody displays an excellent section penetration as confirmed by two previous stereologic studies using the same conditions [25,69] as well as by confocal microscopy.

To explore the relative contribution of neuronal depletion and loss of total number of spinophilin-immunoreactive puncta to cognitive decline, we also obtained stereologic estimates of AD lesions (i.e., total NFT numbers, total amyloid volume) and neuron numbers in the CA1 field in 10 cases (where appropriate material for stereologic counting was available). For stereologic estimates of AD neuronal pathology, floating sections were stained using AT8 (Innogenetics, Gent, Belgium), a monoclonal antibody that recognizes tau proteins phosphorylated at residues Ser199/Ser202 to visualize NFT, NT, and neuritic plaques. Following pretreatment with a solution of 0.25% potassium permanganate and Pal's solution (1% oxalic acid and 1% potassium bisulfite), antibody AT8 was used at a working dilution of 1:3,000 over 24 hours at 4°C. Specific labeling was revealed with an horseradish peroxidase-conjugated anti-mouse antibody (1:100; Dako, Glostrup, Denmark), and 3,3'-diaminobenzidine as a chromogen. The sections were then counterstained with cresyl violet for stereologic determination of unaffected neurons (i.e., neurons stained only by cresyl violet), neurons with intracellular NFT, and extracellular (ghost) NFT [3,6,7,28]. In all cases, antibody AT8 penetrated through the full depth of the sections. Total amyloid volume assessment was made in 50 μm-thick free-floating sections, which were treated with a methanol/H_2O_2 solution (3/1 v/v) for 30 minutes, then washed in phosphate-buffered saline (PBS) for 30 minutes. Subsequently, sections were pretreated with 88% formic acid for 5 minutes to enhance amyloid detection. Incubation with the primary antibody was performed overnight at 4°C, using monoclonal antibody 4G8 (1:3,000; Signet Laboratories, Dedham, MA, USA [5]) diluted in PBS, and 0.5% Triton X-100 and 3% bovine serum albumin. Sections were then rinsed and incubated with biotinylated goat anti-rabbit or goat anti-mouse IgG (H+L) secondary antibody (Vector Laboratories, Burlingame, CA, USA 1:300) for 1 hour. Sections were processed for Nissl staining with cresyl violet, and coverslipped with DePex (Fluka, Milwaukee, WI, USA). All of the staining procedures were already used in our previous stereological studies [3,75].

2.3. Quantitative analysis

The optical fractionator [61] was used to estimate total numbers of spinophilin-immunoreactive puncta in areas CA1 and CA3 of the hippocampus and in area 9. The tissue was sampled in a systematic-random manner from the entire cytoarchitectonically-defined area 9, as previously described [7], and subfields CA1 and CA3 of the hippocampus. All quantitative analyses were performed using a computer-assisted morphometry system consisting of a Zeiss Axioplan 2 photomicroscope equipped with an Applied Scientific Instrumentation MS-2000 XYZ computer-controlled motorized stage, an Optronix MicroFire video camera, a Gateway microcomputer, and the StereoInvestigator morphometry and stereology software (MicroBrightField, Williston, VT). Hippocampal subfields were sufficiently evident in the spinophilin immunohistochemical materials to establish the boundaries of CA1 and CA3. To perform accurate and reliable stereologic analyses in a restricted domain of neocortex it is first necessary to establish the anatomical boundaries of the considered region with as much precision as possible. The materials sampled in the present study were contained within the boundaries established previously [7]. They relied on chemoarchitectonic patterns to recognize the location of Brodmann's area 9 using monoclonal antibody SMI-32 raised against nonphosphorylated neurofilament proteins (Sternberger Monoclonals, Lutherville, MD, USA). This antibody labels a subpopulation of pyramidal neurons in the human neocortex [11,30, 32,48], and has been shown to provide distinct chemoarchitectural characteristics of laminar and region-specific distribution of pyramidal neurons permitting reliable establishment of anatomical boundaries among regional neocortical domains [31,33,52]. The region of the prefrontal cortex referred to as area 9 was characterized by a population of medium to large size pyramidal neurons in layers III and V and a strong labeling of dendrites in the neuropil of these layers. Even though these patterns were perceptible at low magnification, precise outlining of laminar limits was systematically controlled at higher magnification and such patterns remained discernible from adjacent neocortical areas even in demented cases [6,7]. Antibody SMI-32 was used at a working dilution of 1:1,000 on series of sections adjacent to those stained with antibody AD2, and processed as described above. Prior to immunoreaction, all sections for SMI-32 labeling were pretreated in a water bath in 10 mM sodium citrate buffer (pH 6.5) for 10 minutes at 95°C for optimal antigenicity retrieval. SMI-32 immunoreactivity was further enhanced using 0.005% OsO_4. These parallel series of sections were then used as a guide to distinguish the borders of area 9 from adjacent neocortical regions (i.e., Brodmann's areas 8, 46, 10, 32), and permitted an assessment of the variability of the extent of this region and its divergence from classical descriptions. The contours of CA1, CA3, and area 9 were traced at 2.5x magnification as previously described [6,29]. Optical disector counting frames were placed in a systematic-random fashion in the delineated regions of the sections, with constant intervals in the×and y axes. The×and y distances between sampling frames were set at 400 μm in CA1 and CA3, and 250 μm, in area 9. The counting frame width and height were 2 μm. Before counting of total spinophilin-immunoreactive puncta, a pilot study in three randomly selected cases was performed to define the best z-axis thickness of the counting frame in terms of precision of estimates and efficiency. A 2-μm thickness sampling was adopted for stereologic analysis as this pilot study showed that the use of thicker disectors generates additional work without providing substantial benefit in terms of coefficients of error. The area sampling fraction was (2 × 2)/(400 × 400) = 2/160,000 in CA1 and (2 × 2)/(400 × 250) = 4/100,000 in area 9. An oil-immersion objective (100x/1.4 NA) was used for counting. A 2-μm "guard zone" was placed at the top surface of the sections. Counting was performed with the optical disector technique through a depth of 2 μm (the height of dissector). The total spinophilin-immunoreactive profile number in each area was calculated with standard stereologic formulas that are built into the optical fractionator protocols in StereoInvestigator. Coefficients of error (CE) were calculated as previously described [61]. On average, for each hippocampal region 400 labeled puncta were sampled per section, which provided a low CE (range 0.05 – 0.06) and for area 9 approximately 600 puncta per section (CE range 0.06 – 0.09).

The total volume of each analyzed region was estimated using the Cavalieri principle to assess whether changes in the total number of spinophilin-immunoreactive puncta may be due to changes in the volume of each area or changes in the spine density. The profile numbers were quantified in the entire thickness of the cortex [25]. Careful *z*-axis focusing revealed that the immunocytochemical protocol used in the current study yielded high-quality staining with complete penetration of the antibody through the entire section thickness and thus did not interfere with the precision of our estimates that are derived from a small fraction of the nominal tissue thickness.

For stereologic estimates of AD lesions and neurons, the software placed disector frames using a systematic-random design within each contour outlining the cortical layers, to account for a predetermined fraction of the outlined area. This fraction (about 2% in the present study) was established in pilot studies including the full range of CDR scores (0, 0.5, 1, 2, 3) and set to accommodate both sufficient sampling of neurons and NFT and NT, (i.e., 150 to 600 profiles in each case [61,77,78]). Neurons and NFT that fell within these disector frames were then counted. Counting was done at high magnification using a 1.4 n.a. Zeiss Plan-Apochromat 100x objective, and total numbers were estimated using standard formulas [61]. The area of the disector frame was kept at 900 μm^2 for neuron and NFT counts. The total amyloid volume for each region of interest was calculated as $Va_T = (Va_l / V_l) * V_{ref}$ with Va_l being the local amyloid volume determined for each section, V_l the local volume of the region determined for each section, and V_{ref} the volume of reference for an entire region [5].

2.4 Statistical analysis

After normalization of the neuropathologic variables, the relationship between spinophilin-immunoreactive puncta numbers in each area (dependent variable) and Braak NFT stage and Aβ protein deposition staging (independent variables) was studied using linear regression in univariate models. Linear regression models were also used to explore the association between MMSE scores (dependent variable) and neuropathologic parameters (independent variables). The association between CDR scores (as the dependent variable) and neuropathologic parameters (as the independent variables) was studied using maximum likelihood ordered logistic regression which makes it possible to measure the relationship between an ordinal outcome variable (CDR) and several independent variables. Regression models can also evaluate the amount of variability of the outcome variable that can be explained by the independent variables and thus provide an estimate of the strength of the relationship. Statistical analyses were performed using the Stata software package, release 7 (College Station, TX, USA).

3. Results

3.1. Distribution of spinophilin immunoreactivity

Qualitatively, intense spinophilin immunoreactivity was observed in the hippocampus and in all six cortical layers of area 9 as a pattern of bright puncta (~0.5–1 μm in diameter) in both controls and AD patients. Within the CA1 field, the immunostaining was most intense in the stratum oriens and stratum radiatum, weaker in the stratum lacunosum-moleculare, and faint around cell bodies in the stratum pyramidale (Fig. 1A). The pattern of immunoreactivity in the hippocampal formation provided clear boundaries for accurate contours to be drawn in CA1 and CA3 (Fig. 1A). In area 9 the staining pattern was rather homogeneous throughout the cortical layers (Fig. 1B). In contrast, white matter had lower spinophilin staining intensity (Fig. 1). At the magnification at which the quantifications were performed, spinophilin immunoreactivity appeared as a dense punctated pattern in all layers. Whereas stereologic estimates revealed differences among cases, casual observations failed to demonstrate any clear

differences between the local puncta densities between control and AD cases in both the hippocampus and area 9 (Fig. 2).

3.2. Clinicopathologic correlations

Stereologic estimates of spinophilin-immunoreactive puncta are summarized in Table 2. There was a strong negative relationship between Braak NFT stages and total number of spinophilin-immunoreactive puncta in CA1 field ($R = -0.565$, $p < 0.05$) and area 9 ($R = -0.616$, $p < 0.05$) but not in CA3 field ($R = -0.254$, n.s.). In contrast, no relationship was found between Aβ deposition staging and number of spinophilin-immunoreactive puncta in the areas studied (Fig. 3). In a univariate linear regression model, the total number of spinophilin-immunoreactive puncta in CA1 field and area 9 were significantly related to MMSE scores and predicted 23.5% ($p < 0.05$) and 61.9% ($p < 0.001$) of its variability (Fig. 3). Braak NFT staging also explained 59.2% of MMSE variability ($p < 0.001$). The relationship between total number of spinophilin-immunoreactive puncta in CA1 field and MMSE scores did not persist when adjusting for Braak NFT staging in multivariate models. In contrast, the total number of spinophilin-immunoreactive puncta in area 9 was still significantly related to the cognitive outcome explaining an extra 9.6% of MMSE variability. To confirm the validity of these clinicopathologic correlations, we also explored the relationship between number of spinophilin-immunoreactive puncta and CDR scores. There was a clear decrease in the number of spinophilin-immunoreactive puncta across CDR scores. In particular, demented cases (CDR1 and 2) displayed a 14.2% decrease in the CA1 field and 28.2% decrease in area 9 compared to non-demented cases (CDR 0 and 0.5). In a univariate model, total number of spinophilin-immunoreactive puncta in CA1 field and area 9 were negatively related to CDR scores explaining 18% ($p < 0.05$) and 39% ($p < 0.01$) of its variability respectively (Fig. 3). Braak NFT staging was positively related to cognitive decline and predicted 29.9% of CDR scores ($p < 0.01$). As for MMSE scores, the relationship between total number of spinophilin-immunoreactive puncta in CA1 field and CDR scores did not persist after adjusting for Braak NFT staging (34% of CDR variability explained by Braak NFT staging only; $p < 0.05$). In contrast, total number of spinophilin-immunoreactive puncta in area 9 remained a significant predictor of cognitive status explaining an added 25.6% of CDR variability ($p < 0.05$). Interestingly, estimates of spinophilin-immunoreactive puncta in CA3, a region less affected in AD, were not correlated to clinical and neuropathologic indices of AD severity.

The stereologic analysis of AD-related pathology in 10 cases confirmed the observations based on Braak NFT and Aβ staging (Table 3). There was a significant negative relationship between total NFT numbers and total spinophilin-immunoreactive puncta in CA1 field ($R = -0.641$, $p < 0.05$). In contrast, neither total neuron numbers ($R = 0.306$, n.s.) nor total amyloid volume ($R = -0.304$, n.s.) were related to total spinophilin-immunoreactive puncta numbers. In univariate models, total NFT and neuron numbers but not amyloid volume were strongly associated with MMSE score explaining 90.5% and 55.8% of its variability. As for Braak NFT staging, the relationship between total number of spinophilin-immunoreactive puncta in CA1 field and MMSE score did not persist when adjusting for total NFT numbers. Importantly, when both total neuron and spinophilin-immunoreactive puncta in CA1 field were considered, this latter remained an important predictor of the cognitive status explaining an extra 19.6% of MMSE variability.

4. Discussion

The present study reports unbiased stereologic assessment of total spinophilin-immunoreactive profiles in AD cerebral cortex and used multivariate regression models to estimate the contribution of dendritic spine loss in cognitive decline after controlling for the severity of NFT formation. Because synaptic loss may be related to the NFT development in both local

and distally projecting neurons, we used the Braak NFT staging that makes it possible to assess the whole burden of NFT pathology in the brain. Similarly, Aβ protein deposition staging was used to assess the contribution of the fibrillar amyloid burden to the loss of spinophilin-immunoreactive puncta. Three limitations should, however, be considered when interpreting the present data. First, we could not rule out the possibility that potential downregulation of the spinophilin gene expression contributes to our quantitative observations in spines. Second, in the absence of electron microscopy data, it is not possible to exclude that the observed changes in spinophilin immunoreactivity may partly reflect concurrent changes in spine size as suggested in a recent study in macaque monkeys [26]. Third, it was not possible to identify separately cortical layers II–VI in spinophilin-labeled area 9 with the precision required for stereologic analysis. We cannot thus comment on possible laminar differences in AD-related dendritic spine loss within area 9.

Total spinophilin-immunoreactive puncta numbers varied from 3.33 to 6.91 billions in CA1 field, 1.83 to 3.47 billions in CA3 field, and 23.12 to 53.41 billions in area 9. These numbers are significantly lower than those reported in a previous ultrastructural study in the adult rabbit CA1 field (24 billion synapse [22]). This study used an electron microscopy approach to enumerate synapses stereologically and as such obtained estimates of the total number of synapse. It must be kept in mind that our estimate are based on aspine marker that identifies only spines susceptible to receive, mostly, an excitatory contact. Spinophilin immunoreactivity is absent from inhibitory as well as non-spine synapses so that our estimates did not reflect directly the total synapse numbers explaining such discrepancy. In agreement with previous histopathologic studies based on presynaptic markers [57,60], our data failed to identify a relationship between the loss of spinophilin-immunoreactive puncta and Aβ deposition staging. This observation was confirmed in 11 cases with stereologic assessment of total amyloid volumes. Also, consistent with recent animal and human studies, our results point to the necessity to explore the effect of Aβ oligomers in AD-related loss of postsynaptic elements (for review see [12,36,37,55]. The relationship between synaptic loss and NFT burden is still a matter of debate. Although the initial contributions in this field pointed to a possible dissociation between NFT formation and loss of presynaptic markers [68,71], other studies challenged this point of view and postulated a strong relationship between the progression of tau pathology and depletion of synaptophysin [8,10]. Supporting this possibility, Stamer et al. [66] showed that the progressive formation of paired helical filaments might disrupt axoplasmic flow and synaptic survival. Similarly, Callahan et al. [9] documented a progressive reduction of synaptophysin mRNA in single NFT-bearing neurons. In the context of the possible disconnection of corticocortical pathways in AD [30,32,48], dendritic spine pathology is thought to be secondary to abnormal afferent innervation [20,63,65,81]. In line with this hypothesis, Scheff et al. reported in the only stereologic study available in this field a weak positive relationship between NFT densities in layer II of the entorhinal cortex and loss of synaptic contacts in the outer molecular layer of dentate gyrus (i.e. 16% of the synaptic loss was explained by NFT densities), but failed to identify any relationship between the individual's Braak NFT staging and total synaptic numbers in this area [59]. However, this electron microscopy study did not specifically address postsynaptic changes and did not explore synaptic changes in CA1 field and neocortex. Consistent with a direct link between the global NFT burden and postsynaptic damage, our data reveal a strong negative relationship between Braak NFT staging (as well as total NFT numbers in CA1 field) and total numbers of spinophilin-immunoreactive puncta both in the CA1 field and area 9. Importantly, a region-specific vulnerability to both presynaptic and dendritic involvement has been recently described implying that the anatomic correspondence is not the only parameter to consider when interpreting the complex relationships between pre- and postsynaptic changes [39]. It should however be kept in mind that even in our study more than 50% of spinophilin-immunoreactive puncta loss cannot be explained by NFT burden. This finding parallels recent reports of a dissociation between NFT numbers and neuronal loss [38,75] and suggests the

presence of additional non NFT-related determinants of synaptic depletion in AD such as excitotoxic damage and deficient oxidative stress regulation [for review see [58]].

Using both a global neuropsychological measure (MMSE) and a dementia severity scale (CDR), the present study reveals that the loss of dendritic spines in CA1 field and area 9 has a strong negative impact on cognition. This overall observation agrees with several earlier and recent contributions stressing the role of synapses in AD cognitive decline [8,18,28,42,43,58, 59,68,71]. In particular, total numbers of spinophilin-immunoreactive puncta in the CA1 field and area 9 explain more than 20% and 60% of MMSE variability respectively. Unusually high percentages of explained variability (18% for CA1 field and 39% for area 9) were also obtained when the CDR score was used as dependent variable. These values are comparable to those reported in our previous stereologic analysis of total NFT numbers in the CA1 field [75] but significantly higher than those found by Scheff et al. [59] in respect to MMSE scores. As in most previous studies in this field (for review see [23]), our univariate analyses also documented a strong relationship between Braak NFT staging and cognition. This disagrees with the results of Scheff et al. [59] who did not find any relationship between Braak NFT staging and cognition. The overrepresentation of intermediate Braak III stages in their sample is the most plausible explanation for this discrepancy. However, the strong predictive value of spinophilin-immunoreactive puncta counts in CA1 field did not persist when adjusting for Braak NFT staging in multivariate models indicating that the cognitive repercussion of dendritic spine loss in this area is strictly mediated by the global NFT burden. Our quantitative data also confirmed this observation showing that total NFT numbers in this area is the main marker to consider in terms of clinicopathologic correlations. Importantly, they also reveal that the local depletion of pyramidal neurons and loss of spinophilin-immunoreactive puncta are independent phenomena that contribute separately to the cognitive decline. A different pattern was present in area 9 where spinophilin-immunoreactive puncta numbers remained significantly associated with cognitive measures after controlling for Braak NFT staging and explained an additional 9.6% of MMSE variability and 25.6% of CDR variability. These results suggest that neocortical but not hippocampal dendritic spine loss may have an independent cognitive impact in AD. Future clinicopathologic studies in larger series including biochemical analysis of synaptic proteins coupled with stereologic estimates of various presynaptic and postsynaptic markers in the context of defined corticocortical connections between vulnerable areas are needed to assess fully the role of synaptic alterations in brain aging and dementia.

Acknowledgments

We thank Drs Patrick Allen and Paul Greengard for generously providing the anti-spinophilin antibody, and Bridget Wicinski, Ginelle Andrews, and William G.M. Janssen for expert technical assistance. This work was supported by grants AG02219 and AG05138 from the National Institutes of Health, Bethesda, MD (PRH, JHM, DPP, VH), and the Jérôme Tissières Foundation, Geneva, Switzerland (PG).

References

1. Allen PB, Ouimet CC, Greengard P. Spinophilin, a novel protein phosphatase 1 binding protein localized to dendritic spines. Proc Natl Acad Sci USA 1997;94:9956–9961. [PubMed: 9275233]
2. Alzheimer A. Über eine eigenartige Erkrankung der Hirnrinde. Allg Z Psychiat Grenzgeb 1907;64:146–148.
3. Bouras C, Kövari E, Herrmann FR, Rivara CB, Bailey TL, von Gunten A, Hof PR, Giannakopoulos P. Stereologic analysis of microvascular morphology in the elderly: Alzheimer disease pathology and cognitive status. J Neuropathol Exp Neurol 2006;65:235–244. [PubMed: 16651885]
4. Braak H, Braak E. Neuropathological stageing of Alzheimer-related changes. Acta Neuropathol (Berl) 1991;82:239–259. [PubMed: 1759558]
5. Bussière T, Friend PD, Sadeghi N, Wicinski B, Lin GI, Bouras C, Giannakopoulos P, Robakis NK, Morrison JH, Perl DP, Hof PR. Stereologic assessment of the total cortical volume occupied by amyloid

deposits and its relationship with cognitive status in aging and Alzheimer's disease. Neuroscience 2002;112:75–91. [PubMed: 12044473]

6. Bussière T, Giannakopoulos P, Bouras C, Perl DP, Morrison JH, Hof PR. Progressive degeneration of nonphosphorylated neurofilament protein-enriched pyramidal neurons predicts cognitive impairment in Alzheimer's disease: stereologic analysis of prefrontal cortex area 9. J Comp Neurol 2003;463:281–302. [PubMed: 12820162]
7. Bussière T, Gold G, Kövari E, Giannakopoulos P, Bouras C, Perl DP, Morrison JH, Hof PR. Stereologic analysis of neurofibrillary tangle formation in prefrontal cortex area 9 in aging and Alzheimer's disease. Neuroscience 2003;117:577–592. [PubMed: 12617964]
8. Callahan LM, Coleman PD. Neurons bearing neurofibrillary tangles are responsible for selected synaptic deficits in Alzheimer's disease. Neurobiol Aging 1995;16:311–314. [PubMed: 7566340]
9. Callahan LM, Vaules WA, Coleman PD. Progressive reduction of synaptophysin message in single neurons in Alzheimer disease. J Neuropathol Exp Neurol 2002;61:384–395. [PubMed: 12025941]
10. Callahan LM, Vaules WA, Coleman PD. Quantitative decrease in synaptophysin message expression and increase in cathepsin D message expression in Alzheimer disease neurons containing neurofibrillary tangles. J Neuropathol Exp Neurol 1999;58:275–287. [PubMed: 10197819]
11. Campbell MJ, Morrison JH. Monoclonal antibody to neurofilament protein (SMI-32) labels a subpopulation of pyramidal neurons in the human and monkey neocortex. J Comp Neurol 1989;282:191–205. [PubMed: 2496154]
12. Carter J, Lippa CF. Beta-amyloid, neuronal death and Alzheimer's disease. Curr Mol Med 2001;1:733–737. [PubMed: 11899259]
13. Chételat G, Baron JC. Early diagnosis of Alzheimer's disease: contribution of structural neuroimaging. Neuroimage 2003;18:525–541. [PubMed: 12595205]
14. Davidsson P, Blennow K. Neurochemical dissection of synaptic pathology in Alzheimer's disease. Int Psychogeriatr 1998;10:11–23. [PubMed: 9629521]
15. Davies CA, Mann DM, Sumpter PQ, Yates PO. A quantitative morphometric analysis of the neuronal and synaptic content of the frontal and temporal cortex in patients with Alzheimer's disease. J Neurol Sci 1987;78:151–164. [PubMed: 3572454]
16. DeKosky ST, Scheff SW. Synapse loss in frontal cortex biopsies in Alzheimer's disease: correlation with cognitive severity. Ann Neurol 1990;27:457–464. [PubMed: 2360787]
17. Denk W, Yuste R, Svoboda K, Tank DW. Imaging calcium dynamics in dendritic spines. Curr Opin Neurobiol 1996;6:372–378. [PubMed: 8794079]
18. Dickson DW, Crystal HA, Bevona C, Honer W, Vincent I, Davies P. Correlations of synaptic and pathological markers with cognition of the elderly. Neurobiol Aging 1995;16:285–298. [PubMed: 7566338]
19. Dickson DW, Farlo J, Davies P, Crystal H, Fuld P, Yen SH. Alzheimer's disease. A double-labeling immunohistochemical study of senile plaques. Am J Pathol 1988;132:86–101. [PubMed: 2456021]
20. Fiala JC, Spacek J, Harris KM. Dendritic spine pathology: cause or consequence of neurological disorders? Brain Res Rev 2002;39:29–54. [PubMed: 12086707]
21. Folstein MF, Folstein SE, McHugh PR. "Mini-mental state". A practical method for grading the cognitive state of patients for the clinician. J Psychiatr Res 1975;12:189–198. [PubMed: 1202204]
22. Geinisman Y, Gundersen HJ, van der Zee E, West MJ. Unbiased stereological estimation of the total number of synapses in a brain region. J Neurocytol 1996;25:805–819. [PubMed: 9023726]
23. Giannakopoulos P, Herrmann FR, Bussière T, Bouras C, Kövari E, Perl DP, Morrison JH, Gold G, Hof PR. Tangle and neuron numbers, but not amyloid load, predict cognitive status in Alzheimer's disease. Neurology 2003;60:1495–1500. [PubMed: 12743238]
24. Hamos JE, DeGennaro LJ, Drachman DA. Synaptic loss in Alzheimer's disease and other dementias. Neurology 1989;39:355–361. [PubMed: 2927643]
25. Hao J, Janssen WG, Tang Y, Roberts JA, McKay H, Lasley B, Allen PB, Greengard P, Rapp PR, Kordower JH, Hof PR, Morrison JH. Estrogen increases the number of spinophilin-immunoreactive spines in the hippocampus of young and aged female rhesus monkeys. J Comp Neurol 2003;465:540–550. [PubMed: 12975814]

26. Hao J, Rapp PR, Leffler AE, Leffler SR, Janssen WG, Lou W, McKay H, Roberts JA, Wearne SL, Hof PR, Morrison JH. Estrogen alters spine number and morphology in prefrontal cortex of aged female rhesus monkeys. J Neurosci 2006;26:2571–2578. [PubMed: 16510735]
27. Harris KM. Structure, development, and plasticity of dendritic spines. Curr Opin Neurobiol 1999;9:343–348. [PubMed: 10395574]
28. Heinonen O, Soininen H, Sorvari H, Kosunen O, Paljarvi L, Koivisto E, Riekkinen PJ Sr. Loss of synaptophysin-like immunoreactivity in the hippocampal formation is an early phenomenon in Alzheimer's disease. Neuroscience 1995;64:375–384. [PubMed: 7700527]
29. Hof PR, Bussière T, Gold G, Kövari E, Giannakopoulos P, Bouras C, Perl DP, Morrison JH. Stereologic evidence for persistence of viable neurons in layer II of the entorhinal cortex and the CA1 field in Alzheimer disease. J Neuropathol Exp Neurol 2003;62:55–67. [PubMed: 12528818]
30. Hof PR, Cox K, Morrison JH. Quantitative analysis of a vulnerable subset of pyramidal neurons in Alzheimer's disease: I. Superior frontal and inferior temporal cortex. J Comp Neurol 1990;301:44–54. [PubMed: 2127598]
31. Hof PR, Morrison JH. Neurofilament protein defines regional patterns of cortical organization in the macaque monkey visual system: a quantitative immunohistochemical analysis. J Comp Neurol 1995;352:161–186. [PubMed: 7721988]
32. Hof PR, Morrison JH. Quantitative analysis of a vulnerable subset of pyramidal neurons in Alzheimer's disease: II. Primary and secondary visual cortex. J Comp Neurol 1990;301:55–64. [PubMed: 1706358]
33. Hof PR, Mufson EJ, Morrison JH. Human orbitofrontal cortex: cytoarchitecture and quantitative immunohistochemical parcellation. J Comp Neurol 1995;359:48–68. [PubMed: 8557847]
34. Horn G, Bradley P, McCabe BJ. Changes in the structure of synapses associated with learning. J Neurosci 1985;5:3161–3168. [PubMed: 4078621]
35. Hughes CP, Berg L, Danziger WL, Coben LA, Martin RL. A New Clinical Scale for the Staging of Dementia. Brit J Psychiat 1982;140:566–572.
36. Klein WL. Abeta toxicity in Alzheimer's disease: globular oligomers (ADDLs) as new vaccine and drug targets. Neurochem Int 2002;41:345–352. [PubMed: 12176077]
37. Klein WL, Krafft GA, Finch CE. Targeting small Abeta oligomers: the solution to an Alzheimer's disease conundrum? Trends Neurosci 2001;24:219–224. [PubMed: 11250006]
38. Kril JJ, Patel S, Harding AJ, Halliday GM. Neuron loss from the hippocampus of Alzheimer's disease exceeds extracellular neurofibrillary tangle formation. Acta Neuropathol (Berl) 2002;103:370–376. [PubMed: 11904757]
39. Law AJ, Weickert CS, Hyde TM, Kleinman JE, Harrison PJ. Reduced spinophilin but not microtubule-associated protein 2 expression in the hippocampal formation in schizophrenia and mood disorders: molecular evidence for a pathology of dendritic spines. Am J Psychiatry 2004;161:1848–1855. [PubMed: 15465982]
40. Maletic-Savatic M, Malinow R, Svoboda K. Rapid dendritic morphogenesis in CA1 hippocampal dendrites induced by synaptic activity. Science 1999;283:1923–1927. [PubMed: 10082466]
41. Masliah E, Hansen L, Albright T, Mallory M, Terry RD. Immunoelectron microscopic study of synaptic pathology in Alzheimer's disease. Acta Neuropathol (Berl) 1991;81:428–433. [PubMed: 1903014]
42. Masliah E, Mallory M, Alford M, DeTeresa R, Hansen LA, McKeel DW Jr, Morris JC. Altered expression of synaptic proteins occurs early during progression of Alzheimer's disease. Neurology 2001;56:127–129. [PubMed: 11148253]
43. Masliah E, Terry R. The role of synaptic proteins in the pathogenesis of disorders of the central nervous system. Brain Pathol 1993;3:77–85. [PubMed: 8269086]
44. Masliah E, Terry RD, Alford M, DeTeresa R, Hansen LA. Cortical and subcortical patterns of synaptophysinlike immunoreactivity in Alzheimer's disease. Am J Pathol 1991;138:235–246. [PubMed: 1899001]
45. Masliah E, Terry RD, DeTeresa RM, Hansen LA. Immunohistochemical quantification of the synapse-related protein synaptophysin in Alzheimer disease. Neurosci Lett 1989;103:234–239. [PubMed: 2505201]

46. McKinney RA, Capogna M, Durr R, Gahwiler BH, Thompson SM. Miniature synaptic events maintain dendritic spines via AMPA receptor activation. Nat Neurosci 1999;2:44–49. [PubMed: 10195179]
47. Morris JC. The Clinical Dementia Rating (CDR): current version and scoring rules. Neurology 1993;43:2412–2414. [PubMed: 8232972]
48. Morrison JH, Lewis DA, Campbell MJ, Huntley GW, Benson DL, Bouras C. A monoclonal antibody to non-phosphorylated neurofilament protein marks the vulnerable cortical neurons in Alzheimer's disease. Brain Res 1987;416:331–336. [PubMed: 3113670]
49. Moser MB, Trommald M, Andersen P. An increase in dendritic spine density on hippocampal CA1 pyramidal cells following spatial learning in adult rats suggests the formation of new synapses. Proc Natl Acad Sci USA 1994;91:12673–12675. [PubMed: 7809099]
50. Muly EC, Allen P, Mazloom M, Aranbayeva Z, Greenfield AT, Greengard P. Subcellular distribution of neurabin immunolabeling in primate prefrontal cortex: comparison with spinophilin. Cereb Cortex 2004;14:1398–1407. [PubMed: 15217898]
51. Nimchinsky EA, Sabatini BL, Svoboda K. Structure and function of dendritic spines. Annu Rev Physiol 2002;64:313–353. [PubMed: 11826272]
52. Nimchinsky EA, Vogt BA, Morrison JH, Hof PR. Neurofilament and calcium-binding proteins in the human cingulate cortex. J Comp Neurol 1997;384:597–620. [PubMed: 9259492]
53. Ouimet CC, Katona I, Allen P, Freund TF, Greengard P. Cellular and subcellular distribution of spinophilin, a PP1 regulatory protein that bundles F-actin in dendritic spines. J Comp Neurol 2004;479:374–388. [PubMed: 15514983]
54. Perl DP, Good PF, Bussière T, Morrison JH, Erwin JM, Hof PR. Practical approaches to stereology in the setting of aging- and disease-related brain banks. J Chem Neuroanat 2000;20:7–19. [PubMed: 11074340]
55. Rutten BP, Van der Kolk NM, Schafer S, van Zandvoort MA, Bayer TA, Steinbusch HW, Schmitz C. Age-related loss of synaptophysin immunoreactive presynaptic boutons within the hippocampus of APP751SL, PS1M146L, and APP751SL/PS1M146L transgenic mice. Am J Pathol 2005;167:161–173. [PubMed: 15972962]
56. Satoh A, Nakanishi H, Obaishi H, Wada M, Takahashi K, Satoh K, Hirao K, Nishioka H, Hata Y, Mizoguchi A, Takai Y. Neurabin-II/spinophilin. An actin filament-binding protein with one pdz domain localized at cadherin-based cell-cell adhesion sites. J Biol Chem 1998;273:3470–3475. [PubMed: 9452470]
57. Scheff SW, Price DA. Synapse loss in the temporal lobe in Alzheimer's disease. Ann Neurol 1993;33:190–199. [PubMed: 8434881]
58. Scheff SW, Price DA. Synaptic pathology in Alzheimer's disease: a review of ultrastructural studies. Neurobiol Aging 2003;24:1029–1046. [PubMed: 14643375]
59. Scheff SW, Price DA, Schmitt FA, Mufson EJ. Hippocampal synaptic loss in early Alzheimer's disease and mild cognitive impairment. Neurobiol Aging 2006;27:1372–1384. [PubMed: 16289476]
60. Scheff SW, Sparks L, Price DA. Quantitative assessment of synaptic density in the entorhinal cortex in Alzheimer's disease. Ann Neurol 1993;34:356–361. [PubMed: 8363352]
61. Schmitz C, Hof PR. Design-based stereology in neuroscience. Neuroscience 2005;130:813–831. [PubMed: 15652981]
62. Segal M. Dendritic spines: elementary structural units of neuronal plasticity. Prog Brain Res 2002;138:53–59. [PubMed: 12432762]
63. Selkoe DJ. Alzheimer's disease is a synaptic failure. Science 2002;298:789–791. [PubMed: 12399581]
64. Shepherd GM. The dendritic spine: a multifunctional integrative unit. J Neurophysiol 1996;75:2197–2210. [PubMed: 8793734]
65. Spires TL, Meyer-Luehmann M, Stern EA, McLean PJ, Skoch J, Nguyen PT, Bacskai BJ, Hyman BT. Dendritic spine abnormalities in amyloid precursor protein transgenic mice demonstrated by gene transfer and intravital multiphoton microscopy. J Neurosci 2005;25:7278–7287. [PubMed: 16079410]

66. Stamer K, Vogel R, Thies E, Mandelkow E, Mandelkow EM. Tau blocks traffic of organelles, neurofilaments, and APP vesicles in neurons and enhances oxidative stress. J Cell Biol 2002;156:1051–1063. [PubMed: 11901170]

67. Svoboda K, Tank DW, Denk W. Direct measurement of coupling between dendritic spines and shafts. Science 1996;272:716–719. [PubMed: 8614831]

68. Sze CI, Troncoso JC, Kawas C, Mouton P, Price DL, Martin LJ. Loss of the presynaptic vesicle protein synaptophysin in hippocampus correlates with cognitive decline in Alzheimer disease. J Neuropathol Exp Neurol 1997;56:933–944. [PubMed: 9258263]

69. Tang Y, Janssen WG, Hao J, Roberts JA, McKay H, Lasley B, Allen PB, Greengard P, Rapp PR, Kordower JH, Hof PR, Morrison JH. Estrogen replacement increases spinophilin-immunoreactive spine number in the prefrontal cortex of female rhesus monkeys. Cereb Cortex 2004;14:215–223. [PubMed: 14704219]

70. Terry RD, Gonatas NK, Weiss M. Ultrastructural Studies in Alzheimer's Presenile Dementia. Am J Pathol 1964;44:269–297. [PubMed: 14119171]

71. Terry RD, Masliah E, Salmon DP, Butters N, DeTeresa R, Hill R, Hansen LA, Katzman R. Physical basis of cognitive alterations in Alzheimer's disease: synapse loss is the major correlate of cognitive impairment. Ann Neurol 1991;30:572–580. [PubMed: 1789684]

72. Terry RD, Peck A, DeTeresa R, Schechter R, Horoupian DS. Some morphometric aspects of the brain in senile dementia of the Alzheimer type. Ann Neurol 1981;10:184–192. [PubMed: 7283403]

73. Thal DR, Rüb U, Schultz C, Sassin I, Ghebremedhin E, Del Tredici K, Braak E, Braak H. Sequence of Abeta-protein deposition in the human medial temporal lobe. J Neuropathol Exp Neurol 2000;59:733–748. [PubMed: 10952063]

74. Vallet PG, Guntern R, Hof PR, Golaz J, Delacourte A, Robakis NK, Bouras C. A comparative study of histological and immunohistochemical methods for neurofibrillary tangles and senile plaques in Alzheimer's disease. Acta Neuropathol (Berl) 1992;83:170–178. [PubMed: 1373017]

75. von Gunten A, Kövari E, Bussière T, Rivara CB, Gold G, Bouras C, Hof PR, Giannakopoulos P. Cognitive impact of neuronal pathology in the entorhinal cortex and CA1 field in Alzheimer's disease. Neurobiol Aging 2006;27:270–277. [PubMed: 16399212]

76. Weiler R, Lassmann H, Fischer P, Jellinger K, Winkler H. A high ratio of chromogranin A to synaptin/synaptophysin is a common feature of brains in Alzheimer and Pick disease. FEBS Lett 1990;263:337–339. [PubMed: 2110534]

77. West MJ, Østergaard K, Andreassen OA, Finsen B. Estimation of the number of somatostatin neurons in the striatum: an in situ hybridization study using the optical fractionator method. J Comp Neurol 1996;370:11–22. [PubMed: 8797153]

78. West MJ, Slomianka L, Gundersen HJ. Unbiased stereological estimation of the total number of neurons in thesubdivisions of the rat hippocampus using the optical fractionator. Anat Rec 1991;231:482–497. [PubMed: 1793176]

79. Wisniewski HM, Wen GY, Kim KS. Comparison of four staining methods on the detection of neuritic plaques. Acta Neuropathol (Berl) 1989;78:22–27. [PubMed: 2472039]

80. Wolf H, Jelic V, Gertz HJ, Nordberg A, Julin P, Wahlund LO. A critical discussion of the role of neuroimaging in mild cognitive impairment. Acta Neurol Scand 2003;179:52–76.

81. Wong RO, Ghosh A. Activity-dependent regulation of dendritic growth and patterning. Nat Rev Neurosci 2002;3:803–812. [PubMed: 12360324]

82. Yamaguchi H, Hirai S, Morimatsu M, Shoji M, Ihara Y. A variety of cerebral amyloid deposits in the brains of the Alzheimer-type dementia demonstrated by beta protein immunostaining. Acta Neuropathol (Berl) 1988;76:541–549. [PubMed: 3059748]

83. Yuste R, Denk W. Dendritic spines as basic functional units of neuronal integration. Nature 1995;375:682–684. [PubMed: 7791901]

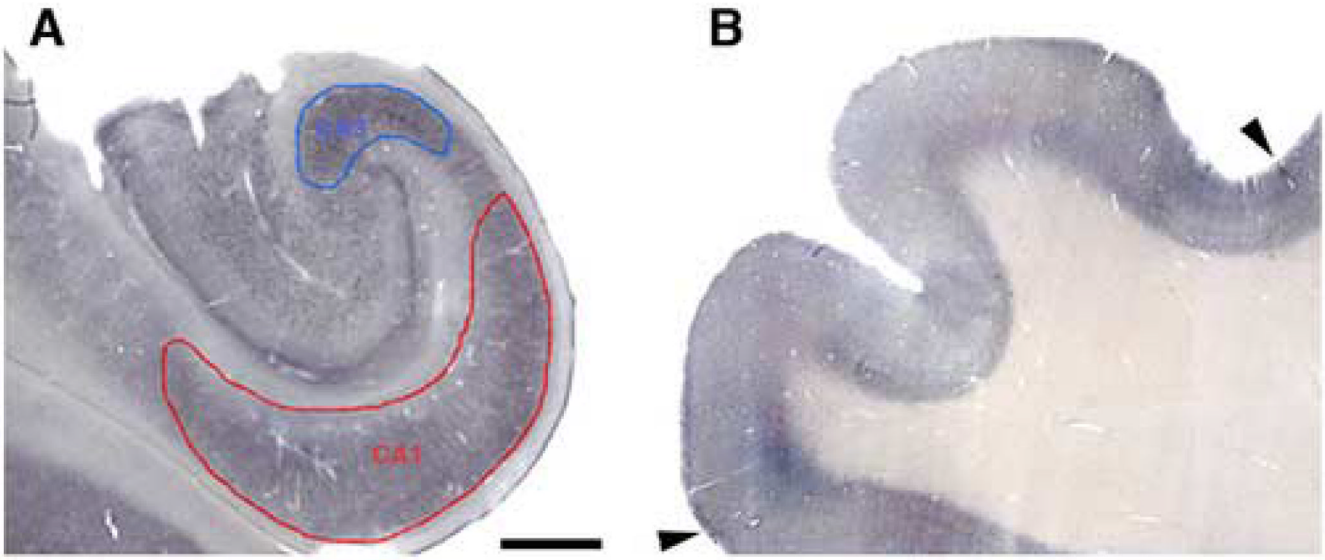

Figure 1.

Photomicrographs of sections through the hippocampus (A) and area 9 (B). A: Coronal section at the level of hippocampus showing the contours of CA1 (red) and CA3 (blue). B: Photomicrograph demonstrating spinophilin labeling in area 9 (arrows mark the boundaries). There is intense spinophilin immunoreactivity in all of the cortical layers, but none in the white matter. Scale bars = 1 mm.

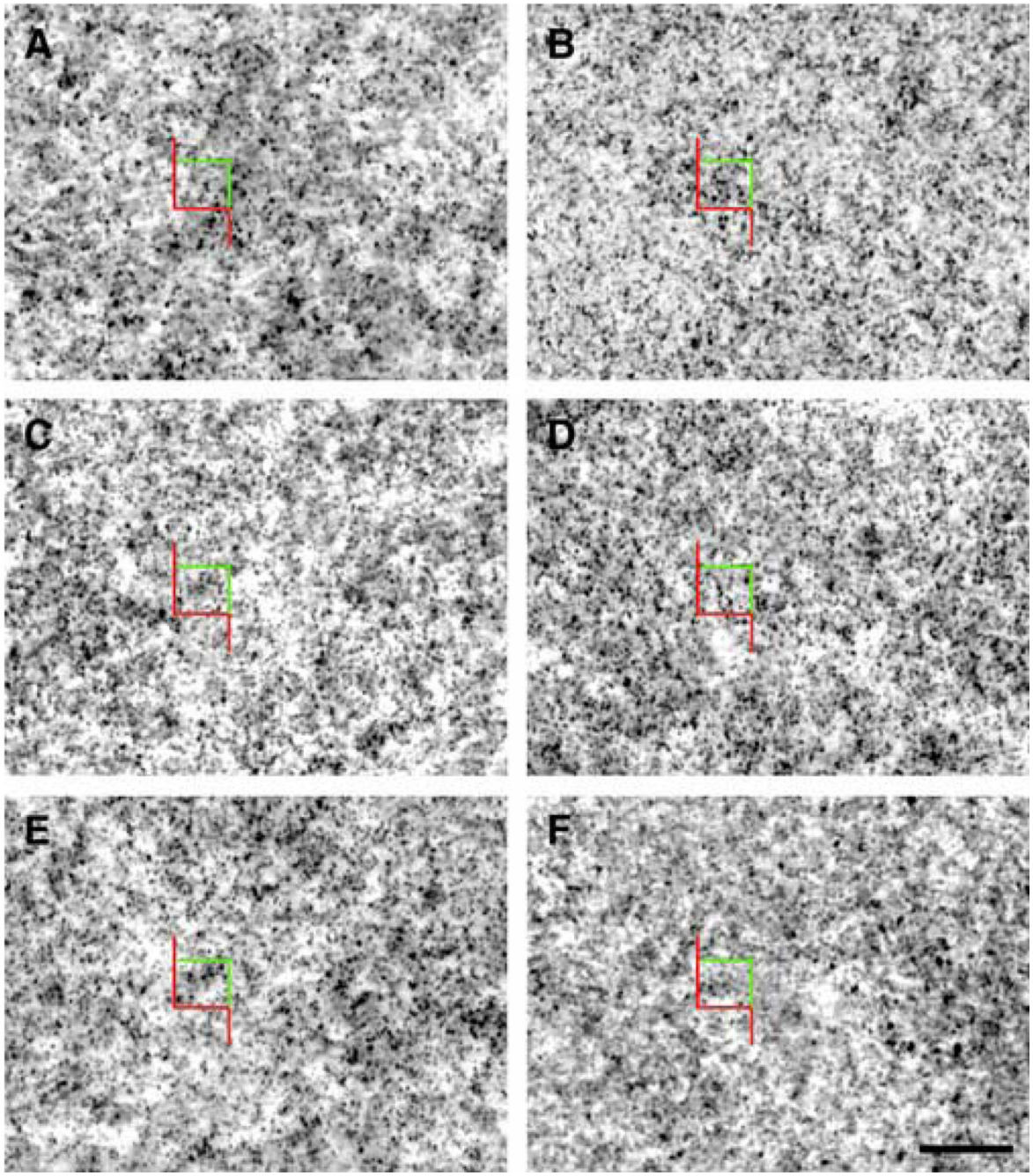

Figure 2.

Photomicrograph showing spinophilin-immunoreactive puncta at 100x magnification (A–F). Spines not visualized at their optimal focal plane appear blurred. (A) Spinophilin immunolabeling in CA1 section (CDR 0) at the magnification used for stereologic analysis. (B) Spinophilin-immunolabeled CA1 section (CDR 3). An unbiased counting frame is shown. The red border of the frame and its extensions represent the exclusion line and the green border represents the inclusion line. Spines were counted when they came into focus within the height of the optical disector and within the counting frame when moving the focal plane continuously through the section. A spine was counted if it was entirely within the counting frame or partially within it without touching or intersecting the exclusion line when in focus. (C, D) High

magnification images of spinophilin immunoreactivity in a CA3 section at CDR 0 and 3 respectively. (E, F) High magnification images of spinophilin immunoreactivity in area 9 at CDR 0 and 2 respectively. Scale bar = 20 μm.

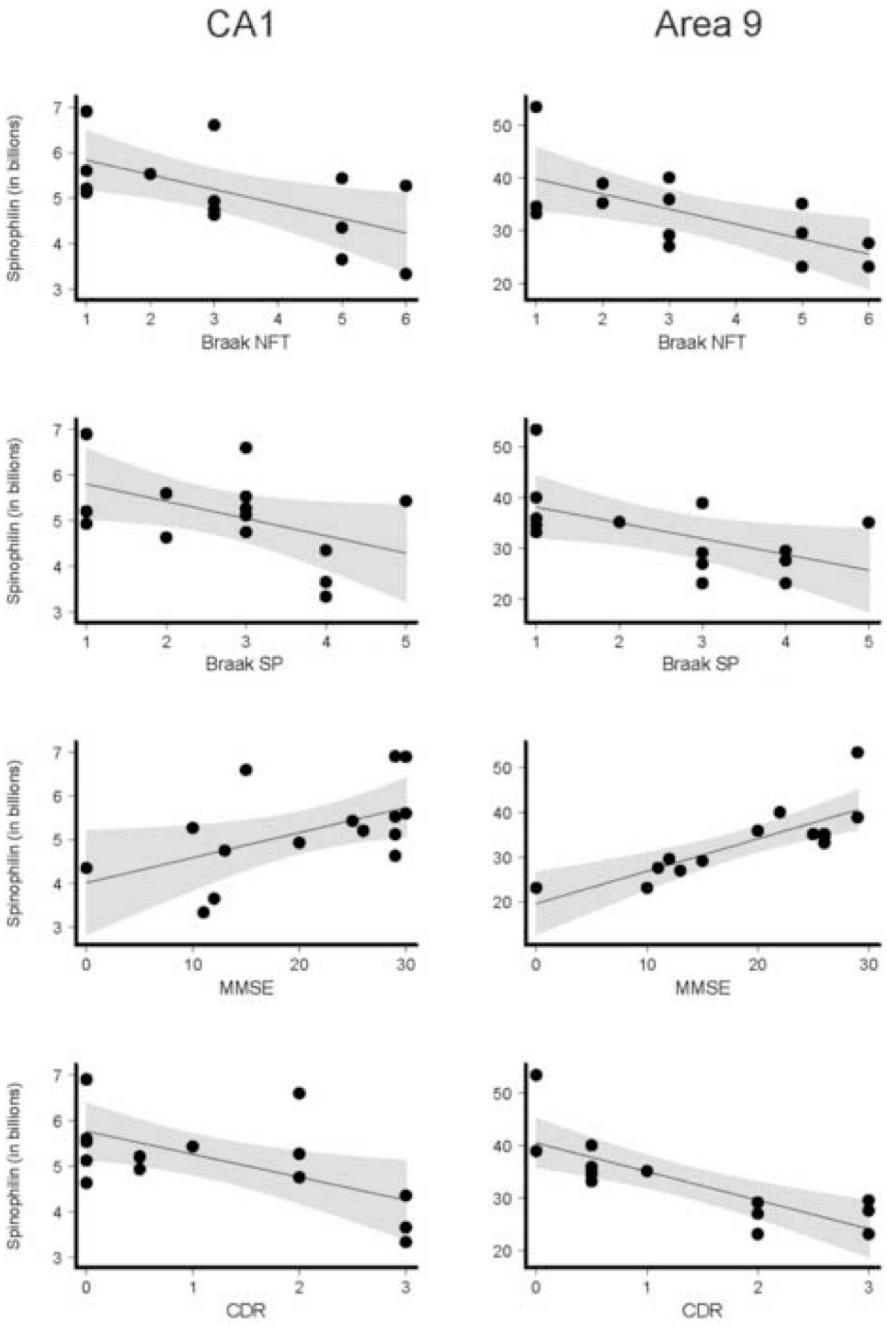

Figure 3.

Regression lines with 95% confidence intervals of spinophilin-immunoreactive puncta (in billions) versus Braak NFT staging, Aβ deposition staging, MMSE, and CDR scores in the CA1 field and area 9. Note the significant negative association between Braak NFT staging and total spinophilin-immunoreactive puncta in both the CA1 field and area 9. Note also the negative relationship between clinical indices and total spinophilin-immunoreactive puncta in the same areas. See text for details.

Table 1

Clinical and demographic data.

No of case	Gender	Age (years)	PMI (hours)	CDR	MMSE	Braak NFT stage	Aβ staging
1	M	74	6	0	29	I	1
2	M	85	7	0	29	II	3
3	W	96	6	0	30	1	2
4	W	97	51	0	29	I	3
5	W	91	25	0	29	III	2
6	M	96	60	0	30	1	1
7	W	61	7	0.5	26	I	1
8	M	85	4.5	0.5	20	III	1
9	M	82	7	0.5	26	I	1
10	M	78	6	0.5	22	III	1
11	M	82	10	0.5	26	II	2
12	W	87	4.5	1	25	II	2
13	W	88	6	2	15	III	3
14	M	88	8	2	13	III	3
15	M	90	2	2	10	VI	3
16	W	83	5	3	12	V	4
17	W	85	11	3	11	VI	4
18	W	95	3	3	0	V	4

PMI, postmortem intrerval; W, woman; M, man; Aβ staging, Aβ deposition staging.

Table 2

Stereologic estimates of the total number of spinophilin-immunoreactive puncta (data represent billions).

Case	CA1	CA3	Area 9
1	6.91	3.15	53.41
2	5.53	2.63	38.91
3	5.60	2.18	n.a.
4	5.12	2.30	n.a.
5	4.63	2.22	n.a.
6	6.90	2.67	n.a.
7	5.20	2.71	33.18
8	4.93	2.16	35.89
9	5.20	3.35	34.55
10	n.a.	n.a.	40.00
11	n.a.	n.a.	35.20
12	5.43	3.34	35.10
13	6.60	2.86	29.14
14	4.75	1.83	27.00
15	5.27	3.47	23.12
16	3.65	1.59	29.55
17	3.33	2.38	27.60
18	4.35	2.06	23.12

n.a., not available.

Table 3

Stereologic estimates of Nissl-stained neuron numbers, NFT numbers, and Aβ deposits volume in the CA1field.

Case	Nissl-stained neurons	NFT	Aß deposits
1	4,856.0	15.0	0
2	7,123.0	12.0	0
3	9,721.6	317.5	13.7
4	6,341.3	764.6	4.1
5	10,727.3	181.7	0.8
6	4,977.4	407.9	2.2
13	3,563.0	1,783.0	23.3
14	2,899.0	2,500.0	11.2
16	2,678.0	3,555.0	9.1
17	2,545.0	3,242.0	144.7

Stereological estimates of total neuron and NFT numbers ($x10^{-3}$) as well as amyloid volume (in mm^3). For case details see Table 1.